Check for updates

Self-flux-grown $Ba_4Fe_4ClO_{9.5−x}$ crystals exhibiting structures with tunable modulation†

Alla Arakcheeva, [iD] *[ab] Wen Hua Bi,[a] Priya Ranjan Baral [iD][a] and Arnaud Magrez [iD][a]

The synthesis and X-ray structural study of the new family of compounds $Ba_4Fe_4ClO_{9.5−x}$ with tunable structural modulation are reported. The framework of the structure has the $Ba_2Fe_4O_{9.5−x}$ composition, with open hexagonal channels extending along the c-axis. The channels are filled with linear [Ba–Cl–Ba] triplets. The oxygen stoichiometry and the oxidation state of iron both are controlled by the redox conditions during crystal preparation. The modulation of the crystal structure arises from the distribution of the oxygen atoms in the framework and iron coordination polyhedra are a combination of FeO_4-tetrahedra, FeO_5-bipyramids, and FeO_6-octahedra. The structure modulation also originates from the ordered or disordered distribution of the [Ba–Cl–Ba] triplets filling the channels which is also affected by the conditions of the thermal treatment of the crystals. The structure investigation reveals a composition variation from $Ba_4Fe_4ClO_{9.5}$ ($x = 0$), in which Fe exhibits a 3+ oxidation state, to $Ba_4Fe_4ClO_8$ ($x = 1.5$) with the framework built exclusively of FeO_4 tetrahedra.

Introduction

Iron-based compounds are an important class of materials for a large spectrum of research areas and applications, including catalysis,[1] energy storage,[2] and magnetic and electric solids/devices.[3,4] Three key factors of iron contribute significantly to these versatilities: the possibility of existing in a wide range of (a) oxidation states and (b) coordination numbers and (c) the ability of iron to bind to a large range of ligands. The oxidation state of Fe varies from 0 in alloys to 6+ in electrochemically grown $MFeO_4$ with M = K_2, Ba, Sr, Cu.[5] The most common oxidation states are Fe^{2+} and Fe^{3+}. Higher oxidation states of Fe are always obtained under special growth conditions which differ from the ones applied in this study. In addition, iron atoms can adopt different coordination numbers, namely 4 (in square planar or tetragonal geometry) and up to 8 (in dodecahedral or pseudo-cubic geometry). The prevalent coordination polyhedra are tetrahedron, octahedron, and trigonal Fe-bipyramid.[6,7] Among the plethora of Fe-based compounds, about 150 inorganic or organic–inorganic hybrid oxychlorides can be found in the

ICSD and COD databases.[8,9] FeOCl, the simplest iron oxychloride, exhibits a two-dimensional structure.[10] Structure and Fe oxidation state are controlled by the intercalation of organic molecules or of alkali atoms between the well-separated layers of FeOCl.[11]

Among the two known examples of barium-containing iron oxychlorides, $Ba_3Fe_2O_5Cl_2$ is a chiral insulating magnet crystallizing in the cubic space group $I2_13$.[12] The Fe^{3+}-containing corner-sharing tetrahedra form pseudo two-dimensional 10-membered rings. This compound undergoes an antiferromagnetic (AFM) transition (T_N) at 564 K and shows an AFM to weak ferromagnetic transition (T_S) at 140 K, accompanied with a structural distortion. In the second example, $10H–BaFeCl_{0.13}O_{3−y}$, cubic and hexagonal layers are stacked in the *hhchc* order.[13] While chlorine is located only in the hexagonal layer, oxygen vacancies are distributed over both layers. The iron atoms are located in face-sharing octahedra as well as in dimers of corner-sharing tetrahedra. $10H–BaFeCl_{0.13}O_{3−y}$ has a T_N of 730 K and undergoes an AFM to ferrimagnetic transition below 400 K. The high-temperature magnetism makes the barium iron oxychlorides interesting from the magnonics point of view, among other potential applications.[14]

Herein, we report on the synthesis and structural characterization of a new barium iron oxychloride. $Ba_4Fe_4ClO_{9.5−x}$ crystals with mixed-valence iron (2+/3+) are synthesized as black needles (Fig. 1), exhibiting a modulated crystal structure. Based on detailed single-crystal X-ray diffraction (XRD) data, we found $Ba_4Fe_4ClO_{9.5−x}$ to exhibit a modulated crystal structure with modulations depending on

a SB, IPHYS, Crystal Growth Facility, Ecole Polytechnique Fédérale de Lausanne, Lausanne 1015, Switzerland. E-mail: alla.arakcheeva@epfl.ch, allaarakcheeva@gmail.com, arnaud.magrez@epfl.ch
b Phase Solutions Co Ltd, ch. des Mésanges 7, Lausanne 1012, Switzerland
† Electronic supplementary information (ESI) available: Reconstructions of the reciprocal space sections; indexing of reflexions; simulated and experimental XRD profiles; tables of experimental details for structure determination and refinements; atomic position parameters for average structures. See DOI: 10.1039/d1ce01657a
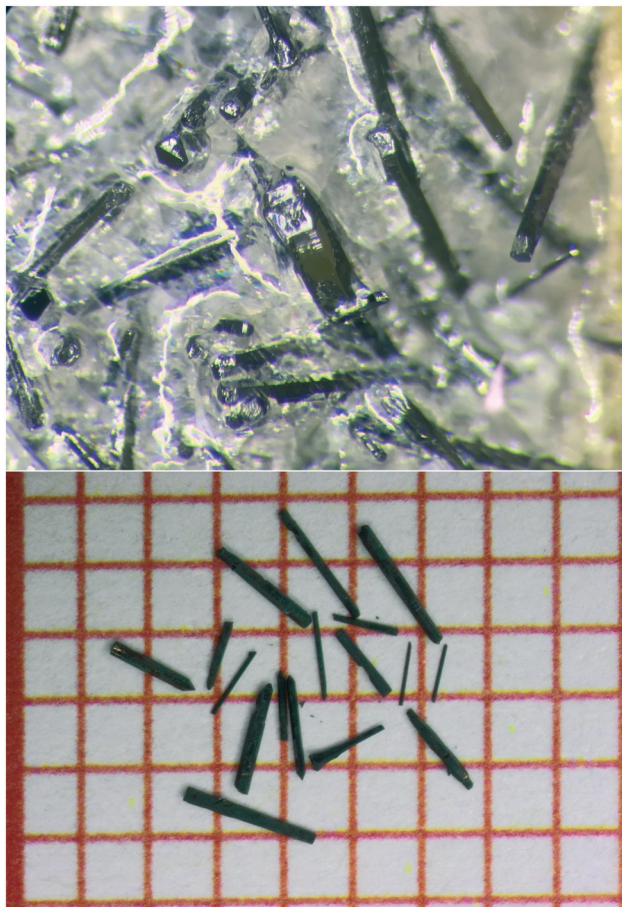
Fig. 1 (Top) As-grown $Ba_4Fe_4ClO_{9.4(1)}$ crystals in $BaCl_2$ flux. (Bottom) $Ba_4Fe_4ClO_{9.0(1)}$ crystals, annealed at 800 °C in an Ar/H_2 flow, on a grid paper. The spacing between the lines is 1 mm.

the conditions of crystal growth and post-growth annealing. The iron atoms are found to be in tetrahedral, bipyramidal as well as octahedral coordination by O atoms. The large hexagonal channels formed by the structure framework are filled with [Ba–Cl–Ba] linear triplets, which are mobile. Their distribution is influenced by the annealing conditions. In addition to the magnetic properties, such an open framework compound with potentially replaceable fillers could be interesting for chemical separation, for synthesis as well as for catalysis.

Experimental

Growth of $Ba_4Fe_4ClO_{9.5-x}$ crystals

Single crystals of $Ba_4Fe_4ClO_{9.5-x}$ were prepared in a $BaCl_2$ flux. $BaCO_3$, $FeC_2O_4 \cdot 2H_2O$, and $BaCl_2$ were mixed in a ratio of $2:2:10$. The mixture was transferred into an alumina crucible and heated at 1000 °C for 24 hours. After cooling from 1000 °C to 900 °C at a rate of 1 °C h^{-1}, the mixture was quenched to room temperature. In a typical growth experiment, 3.1707 g of $FeC_2O_4 \cdot 2H_2O$, 3.4781 g of $BaCO_3$ and 18.3513 g of $BaCl_2$ are mixed. From this mixture, about 1.5 g of $Ba_4Fe_4ClO_{9.5-x}$ crystals are obtained which corresponds to

a yield of approximately 33%. The $BaCl_2$ excess used as flux was subsequently washed with deionized water. The entire growth process proceeded in air. Crystals are stable in air and in water.

As shown in Fig. 1, black needles with lengths of up to a few millimetres were obtained. The Ba/Fe/Cl stoichiometry is confirmed to be 4.00(4)/4.0(2)/1.0(1), by X-ray fluorescence (XRF).

Annealing of $Ba_4Fe_4ClO_{9.5-x}$ crystals in different conditions

In order to modify the oxygen stoichiometry and concurrently the oxidation state of Fe, the needles were annealed in different conditions: (i) in air at 400 °C for 16 hours, (ii) in a continuous flow of O_2 (20 sccm) at 500 °C for 16 hours, (iii) in vacuum (0.1 mbar) at 800 °C for 16 hours, (iv) in an Ar/H_2 flow (80 sccm/20 sccm) at 500 °C for 16 hours.

The needles remained unchanged after annealing (Fig. 1). Independently of the redox conditions, the composition 4.0(2)/4.0(1)/1.00(3) was confirmed by XRF measurements.

XRF experiments

XRF measurements were performed using an OrbisPC Micro EDXRF analyzer system, equipped with a Rh micro-focus X-ray tube (50 kV and 1 mA), a 30 μm poly-capillary X-ray optics, and an Apollo XRF-ML50 silicon drift detector with an energy resolution lower than 135 eV. All the XRF measurements reported here were performed under vacuum conditions.

XRD experiments

Crystals with suitable size were selected and mounted on a goniometer head with cryo-loops. All data sets were collected at room temperature and 100 K using a Rigaku Synergy-I XtaLAB X-ray diffractometer, equipped with a Mo micro-focusing source (λK_α = 0.71073 Å) and a HyPix-3000 hybrid pixel array detector. The temperature was controlled by a Cryostream 800 from Oxford Cryosystems Ltd. CrysAlisPRO[15] and JANA2006 software[16] were used for the processing of raw experimental data and structural refinements, respectively. Structure solutions were obtained with the Superflip program.[17] Other experimental details are listed in Tables S1 and S2.† Further experimental details are available as CIF files with CSD numbers 2126985–2126989 for the average structure and with CSD numbers 2127041 and 2127080 for the modulated structures. The DIAMOND program from Crystal Impact was used to draw the crystal structures.[18]

Results and discussion

The crystal structures of the as-grown crystals and those annealed under different redox conditions have been analyzed by using: (i) reciprocal space reconstructions based on the single-crystal XRD experiments; (ii) refinements of the average structure for the modulated crystals; and (iii) refinements of the modulated structures using the superspace symmetry and a supercell presentation when possible.

Analyses of the XRD reciprocal space reconstructions

Reconstruction of the reciprocal space cross sections, which are typical for crystals prepared under different redox conditions, is shown in Fig. 2 and with more details in Fig. S1.† Three different groups can be distinguished. Group **I** (Fig. 2) includes the crystals prepared under oxidizing or neutral conditions, namely as-grown crystals, crystals annealed in O_2, in air and in vacuum at $T < 600$ °C. Group **II** (Fig. 2) corresponds to the crystals annealed in vacuum at $T > 800$ °C. Crystals belonging to these two groups have similar composition, *i.e.* $Ba_4Fe_4ClO_{9.4(1)}$, but different crystal structure modulation. Group **III** (Fig. 2) contains crystals annealed under reducing atmosphere (Ar + H_2). The oxygen stoichiometry of group **III** crystals is reduced to 9.0(1).

Four significant conclusions can be drawn from the observations of the XRD patterns.

– First, all the patterns point towards hexagonal symmetry of the crystals, irrespective of the group.

– Second, the strongest reflections observed for all patterns are identical. They define the basic hexagonal unit cell ($a = b \approx 5.77$ Å and $c \approx 10.0$ Å) with the reciprocal parameters a^*, b^* and c^* shown in Fig. 2.

– Third, the system of the weaker satellite reflections resulting from structure modulations is specific for each group. Namely, the satellite reflections for groups **I** and **II** suggest some modulations only in the hexagonal plane (Groups **I** and **II**, Fig. 2), while the satellite reflections of group **III** indicate an additional modulation along the *c*-axis (0*kl* cross sections in Fig. 2).

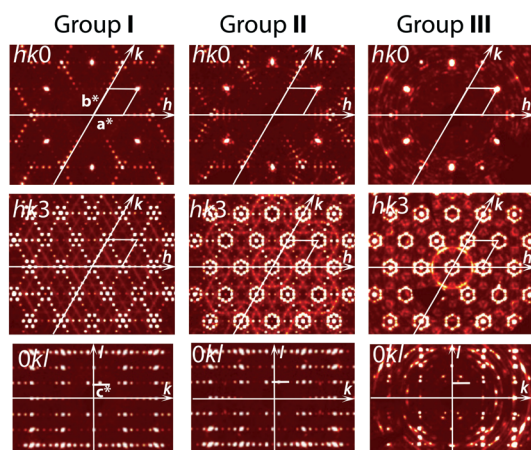– Fourth, crystals belonging to these three groups can readily be distinguished by partial atomic disorder in their modulated structures. This is proved by the significant difference in diffuse scattering between the three groups (Fig. 2; more details can be seen in Fig. S1 and S2†).

Average structure determination and description

The average structure with the hexagonal unit cell parameters $a \approx 5.77$ Å and $c \approx 10.0$ Å was initially refined in the $P6_3/mmc$ space group for all the crystals. However, the presence of weak, but clearly visible reflections 00*l* and *hhl* with $l = 2n + 1$ for all the crystals, contradict the 6_3-screw axis and the *c* glide plane, respectively. Consequently, lower symmetries were tested, and the best solution was obtained with the $P\bar{6}m2$ space group with the best reliability factor $R_I = 0.032$–0.040. Experimental details for the average structure determination and refinement of $Ba_4Fe_4ClO_{9.5-x}$ are listed in Table S1† for crystals of groups **I**, **II** and **III**. The refinement results point to an oxygen stoichiometry which is group dependent. As expected from the growth and annealing conditions, crystals treated in oxidizing or neutral atmosphere (groups **I** and **II**) present a higher oxygen stoichiometry, $x = 9.4(1)$, than that of group **III** crystals, $x = 9.0(1)$, treated in reducing atmosphere.

Fig. 3 shows a sketch of the average structure. The atomic sites of the structure are shown in Fig. 3a; details are listed in Table S3† for crystals prepared at different conditions. The main framework of the structure is made of Fe-polyhedra sharing vertices and faces. Half of Ba atoms are embedded in this framework of $Ba_2Fe_4O_{9.5-x}$ composition. The rest of the Ba atoms and Cl atoms are located in hexagonal channels (Fig. 3b). The atomic sites of the framework are fully occupied, with the exception of O22a and O22b at $z = 0$, and O21a and O21b at $z = 0.5$. For both $z = 0$ and $z = 0.5$, the oxygen "a" and "b" sites can only be alternately occupied due to the short 1.5 Å distance between them (red color in Fig. 3a). However, at least one O atom either "a" or "b" must be present at both $z = 0$ and $z = 0.5$ in order to complete the coordination polyhedron for
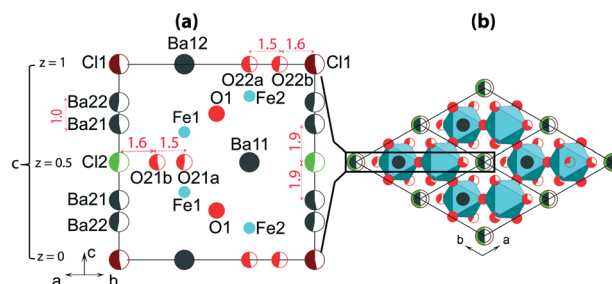

Fig. 2 Representative cross sections of the reciprocal space reconstruction for $Ba_4Fe_4ClO_{9.5-x}$ crystals treated under different redox conditions. Vertical panels "Group I", "Group II" and "Group III" refer to the redox conditions during the crystal growth and post-growth annealing. Sections *hk*0, *hk*3, 0*kl* reveal the brightest main reflections, weaker satellite reflections, and specific features of diffuse scattering. The main reflections define the average reciprocal unit cell (white rhombuses for a^*, b^* in *hk*0 and *hk*3 and white dash for c^* in 0*kl* sections), which is identical for all the crystals.

Fig. 3 Sketch of the disordered average structure of $Ba_4Fe_4ClO_{9.5-x}$ and estimation of an atomic ordering in a hypothetical modulated structure. Panel (a) shows the (1 −1 0) cross section containing all atomic sites in the average structure. Incompletely filled circles indicate partially occupied sites. Red indicates unacceptable short interatomic distances (Å) leading to partial site occupancy. Panel (b) shows a projection of the average structure along the *c*-axis; Fe-polyhedra are emphasised in blue. Four unit cells are illustrated with black lines.

each of the Fe atoms. The expected polyhedra are FeO_4-tetrahedron, FeO_5-bipyramid or FeO_6-octahedron. The partial ordering of these O atoms is one of the main reasons for the formation of modulated structures.

Another possible reason for the structural modulation is the ordering of the filler in the channels, where the Ba- and Cl-sites are only partially occupied due to the short interatomic distance between them (red color in Fig. 3a). Cl1 and Cl2 can only be associated with two Ba21 and two Ba22, respectively, with Cl–Ba distance close to 3 Å, so that the channels can locally contain either [Ba21–Cl1–Ba21] or [Ba22–Cl2–Ba22] triplets. According to the refinement, the occupation of each triplet is close to 0.5 (Table S3†) corresponding to a total of one triplet per unit cell. An ordered distribution of the triplets can only be achieved in a modulated structure, the existence of which is confirmed by satellite reflections in the reciprocal space maps. The presence of diffuse scattering, as shown in Fig. 2, and S1 and S2,† points towards partial disorder in the distribution of the triplets.

Prediction of crystal compositions with unmodulated structure

In the following paragraphs, possible prototypes of completely ordered structures compatible with the average structure model without modulation are discussed.

The first prototype is based on a framework built exclusively with FeO_4 tetrahedra (right-hand sub-cell in Fig. 4). The corresponding chemical formula $Ba_4Fe_4ClO_8$ imposes a ratio of 1/3 between Fe^{3+}/Fe^{2+}. A higher Fe^{2+} content, corresponding to an O stoichiometry lower than 8, is not possible as Fe cannot accommodate a coordination number lower than 4. We hypothesise that $Ba_4Fe_4ClO_8$ could be produced in highly reducing conditions to maintain the average 2.25 oxidation state of Fe.

The second prototype is $Ba_4Fe_4ClO_9$ (left-hand sub-cell in Fig. 4). Two out of the four tetrahedra are replaced by edge-sharing FeO_5 trigonal bipyramids. The prototype composition imposes the Fe^{3+}/Fe^{2+} ratio to be 3/1.

The framework composition and its charge in the Ba_4Fe_4-ClO_8 and $Ba_4Fe_4ClO_9$ structures, $[Ba_2Fe_3^{2+}Fe_1^{3+}O_8]^{3-}$ and $[Ba_2$-$Fe_1^{2+}Fe_3^{3+}O_9]^{3-}$, respectively, are compatible with the presence of one $[Ba–Cl–Ba]^{3+}$ triplet per unit cell in the hexagonal channels.

The maximum oxygen stoichiometry of 9.5 is obtained with all Fe atoms having the 3+ oxidation state. The corresponding framework with the $[Ba_2Fe_4^{3+}O_{9.5}]^{3-}$ formula would also accommodate one $[Ba_2Cl]^{3+}$ triplet per unit cell in the channels. This is confirmed experimentally by the average structure refinement of crystals from both groups **I** and **II** resulting in a composition close to $Ba_4Fe_4ClO_{9.5}$. However, the oxygen distribution cannot be completely ordered because of the short O–O as well as Ba–Cl distances as discussed in the average structure description. As concluded from the average structure refinement, the structure requires a description in a supercell or with an incommensurately modulated model. An example of a hypothetical $5a \times 5b \times 1c$ supercell is shown in Fig. 4. It corresponds to a modulated structure with an average oxygen stoichiometry close to 9.5.

In conclusion, the stoichiometry of $Ba_4Fe_4ClO_{9.5-x}$ is limited to $0 \leq x \leq 1.5$. In the structures, a partial disorder in the distribution of the O atoms as well as the [Ba–Cl–Ba] triplets is also possible. This is discussed in more details in the following section, along with the analysis of the diffuse scattering observed in the XRD patterns.

Structural order/disorder *versus* crystal treatments

As can be observed in Fig. 2 and S1 and S2,† the diffuse scattering depends on the crystal post-growth processing conditions. The evolution of this diffuse scattering as seen by comparing the XRD patterns of groups **I** and **II** (annealed at 600 °C *versus* 800 °C) confirms a higher structural disorder by increasing annealing temperature in either oxygen-containing or neutral atmosphere. On the other hand, an opposite effect is seen when crystals are annealed under reducing atmosphere. Diffuse circular lines characteristic of groups **I** and **II** in *hk*3 reciprocal plane transform into diffuse maxima which are characteristic of group **III**. This means that annealing under reducing atmosphere tends towards an improved ordering of the [Ba–Cl–Ba] triplets in the channels as well as of the O atoms in the atomic planes perpendicular to the hexagonal *c*-axis.

The residual electron density maps calculated from the average structure refinement (Fig. 5) confirm the conclusions drawn from the diffuse scattering analysis. Moreover, they provide additional information for understanding the atomic order/disorder.

In Fig. 5, the positions of Ba and Cl atoms in the channels and O atoms in the framework are shown in the maps of the residual electron density. For group **I** (Fig. 5), a weak density
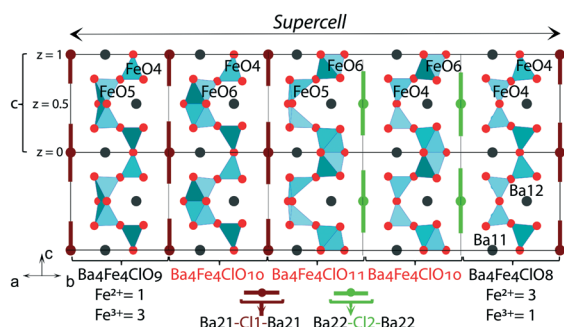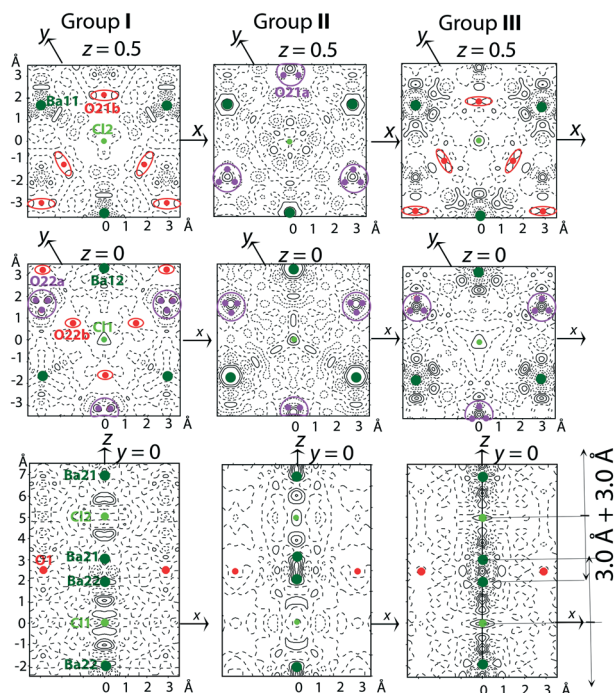

Fig. 4 Possible atomic ordering in a hypothetical supercell ($5a \times 5b \times 1c$) of the modulated structure with a composition close to $Ba_4Fe_4ClO_{9.5}$. The particular combination of different Fe polyhedra which characterizes each sub-cell in the supercell leads to its specific composition, which is indicated below each sub-cell with red or black colour. Only the sub-cells named with a black colour emphasise a combination of Fe polyhedra and composition which would give a non-modulated and fully ordered structure. The sub-cells with a red colour cannot exist alone. They need to be combined with other sub-cells in black in a supercell model.

Fig. 5 The residual electron density calculated after the average structure refinement for $Ba_4Fe_4ClO_{9.5-x}$ crystals treated under different redox conditions. Groups **I**, **II** and **III** (vertical panels) are represented by data from the crystals annealed at 400 °C in air, 800 °C in vacuum and 500 °C in an Ar/H_2 flow, respectively. Solid, dashed and dotted contours correspond to positive, zero and negative values of electron density; the contour step is 0.5 e $Å^{-3}$. Refined atomic positions are shown in different colours for Ba (dark green), Cl (light green), O (red and purple). The split positions of the O atoms are outlined by ellipses.

wave of ±0.5 e $Å^{-3}$ in the vicinity of Ba11 and Ba12 atoms indicates an anharmonic atomic displacement (ADP). In the channels, broad maxima between Ba21, Ba22, Cl1 and Cl2 point to some disorder in the distribution of [Ba–Cl–Ba] triplets. The weak maxima of 0.5 e $Å^{-3}$ near O21b and split O22b can be associated with a statistical displacement of the atoms or a position modulation of the sites which are partly vacant.

For group **II** (Fig. 5), the main difference from group **I** is an increase in the disordered distribution of [Ba–Cl–Ba] triplets in the channels. The triplet disorder affects the disorder of O atoms at $z = 0$ and $z = 0.5$ due to the Cl–O distance, which should be about 3.0 Å.

For group **III** (Fig. 5), the sharp maxima between Ba and Cl atoms indicate that both the triplet occupancy and position modulation in the channels are possible. In addition, some order of the triplet distribution along the c-axis is confirmed by the presence of satellite reflections in the $0kl$ sections of the reciprocal space (group **III** in Fig. 2).

The conclusions of the diffuse scattering characteristics (Fig. 2 and S1 and S2†) and the residual electron density (Fig. 5) analysis can be summarized as follows: (i) the distribution of [Ba–Cl–Ba] triplets in the channels contributes to both the structural modulations (ordering of the triplets) and diffuse scattering (disordering of the triplets); (ii) structural disorder increases with an increase in the crystal

post-growth processing temperature under oxidizing and neutral conditions; (iii) the reduction of the oxygen stoichiometry imposed by the annealing in reducing atmosphere improves the ordering of the structure.

Superspace group determination for compounds treated in different conditions

Based on the unit cell of the average structure and consideration of the satellites, the following superspace groups are determined.

For crystals of group **I**, two modulation vectors, $q1 = 1/5a^*$ and $q2 = 1/5b^*$, were found. Fig. 6 (see also Fig. S3a†) illustrates the reflection indexing. The absence of satellite extinction determines a unique (3 + 2)-dimension superspace group $P\bar{6}m2$ $(\alpha,0,0)000(-\alpha,\alpha,0)00$ (No. 187.2.82.3).[19] The value of $\alpha = 1/5$, obtained as a result of the q-vector refinements during the integration of reflections, points to a commensurately modulated structure, which is therefore described with the hexagonal unit cell parameter $a' = a \times 5 = 5.77 \times 5 = 28.5$ Å.

For group **II** crystals (Fig. 6, group **II**), additional weak reflections impose two additional q-vectors, $q1' = 1/15a^* + 1/15b^*$ and $q2' = -2/15a^* + 1/15b^*$, which are related to the previous ones as $q1' + q2' = q1$ and $2q2' + q1' = q2$. Fig. 6, group **II** (see also Fig. S3b†) illustrates the relationship between the q-vectors and the indexation of reflections. Correspondingly, the superspace group was identified as (3 + 2)-dimension $P\bar{6}m2$ $(\alpha,\alpha,0)000(-2\alpha,\alpha,0)00$ (No. 187.2.83.4).[19] The value of the refinement coefficient $\alpha = 1/15$ points to the commensurately modulated hexagonal structure with $a = 5.77 \times 15 = 85.5$ Å.

The reciprocal space structure of group **III** is characterized by more complex patterns of satellite reflections (Fig. 7 and S4†).

In addition to the satellites defined by the refined vectors $q1'' = 1/16a^* + 1/16b^*$ and $q2'' = -2/16a^* + 1/16b^*$, which are similar to $q1'$ and $q2'$, a third vector $q3 = 1.277c^*$ appears. It indicates additional structure modulation along the

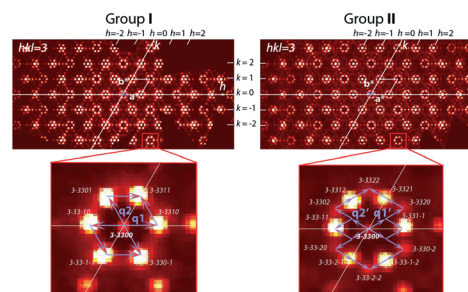**Fig. 6** Indexing of reflections for $Ba_4Fe_4ClO_{9.5-x}$ in crystal groups **I** and **II**. For group **I**, the vectors of commensurate modulation are $q1 = 1/5a^*$ and $q2 = 1/5b^*$. For group **II**, the vectors of commensurate modulation, $q1' = 1/15a^* + 1/15b^*$ and $q2' = -2/15a^* + 1/15b^*$, are related to the previous vectors as $q1' + q2' = q1$ and $2q2' + q1' = q2$. The $hklmn$ index of each reflection is defined by the vector sum $ha^* + kb^* + lc^* + mq1 + nq2$ and $ha^* + kb^* + lc^* + mq1' + nq2'$ for groups **I** and **II**, respectively.
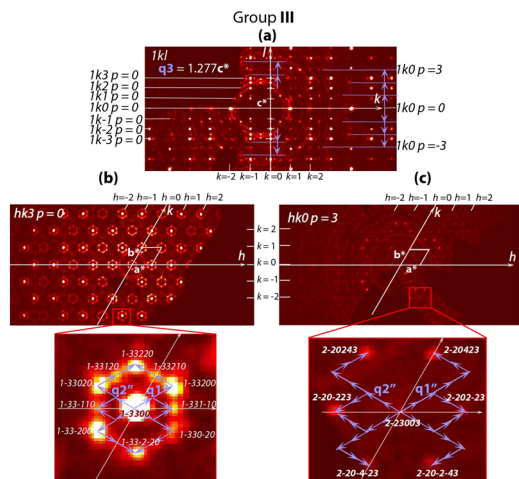
Fig. 7 Indexing of reflections for the $Ba_4Fe_4ClO_{9.5-x}$ crystal of group **III**. Panel (a): Cross section 1kl shows the incommensurate vector $\pm q3 = 1.277c^*$ applied to reflection lines 1k0 and 1$k \pm 2$. Panel (b) shows reflections that can be indexed in hk3 planes using the commensurate modulation vectors $q1'' = 1/16a^* + 1/16b^*$ and $q2'' = -2/16a^* + 1/16b^*$ as shown at the bottom. Panel (c) shows satellite reflections, which can be only indexed using the additional $q3$ vector as shown at the bottom. The $hllmnp$ indexation uses the vector sum: $ha^* + kb^* + lc^* + mq1'' + nq2'' + pq3''$.

hexagonal c-axis. The satellite diffraction spots and those assigned to the average structure (Fig. 2 and 7 and S4†) are consistent with the (3 + 3)-dimension superspace group $P\bar{6}m2$ $(\alpha,\alpha,0)000(-2\alpha,\alpha0)000(00\gamma)000$ (No. 187.3.200.3)[19] with the commensurate coefficient $\alpha = 1/16$ and incommensurate coefficient $\gamma = 1.277$. Accordingly, $a = 5.77 \times 16 = 93.3$ Å.

Refinement of the $Ba_4Fe_4ClO_{9.5-x}$ modulated structures

Using the identified superspace group, the commensurately modulated structure was refined for as-grown crystals at 100 K (group **I**). The refinement resulted in rather good characteristics: $R(all) = 0.050$; $wR_2(all) = 0.117$; $R(main) = 0.030$; $wR_2(main) = 0.072$. However, the harmonic approximation needs to be applied to refine the occupancy

modulation of the [Ba–Cl–Ba] triplets, as well as the O atoms. The refined occupancy varies continuously from −0.7 to 1.3 which does not provide accurate information about the occupation of either the triplets or the O21 and O22 atoms.

Therefore, the supercell approximation was imposed for the structural refinement in order to estimate the O atom occupancy and, as a consequence, the oxidation state of Fe atoms. The refinement of the supercell structure was successful for the as-grown crystals and the ones annealed at 400 °C in air, at 500 °C in O_2, as well as at 550 °C in vacuum. As seen in Fig. 8, the a lattice parameter is 5 times larger than that of the average structure. The details of our structural refinements given in Table S2† include the as-grown crystal using both the superspace and supercell approach, and for a crystal annealed at 400 °C in air using the supercell approximation. A CIF file corresponding to the refinement for the as-grown crystal using the supercell approximation is available with CSD number 2127041 as a representative example for group **I**. Illustrations of the structure are shown in Fig. 8a and b.

It can be seen that the distribution of the [Ba–Cl–Ba] triplets is partially ordered. However, the alternate occupancy of the triplets along the c-axis confirms the distribution to be partially disordered which is evident from the diffusion scattering observed in the reciprocal space reconstructions (Fig. 2, group **I**; and S1 and S2†). The refined chemical formula $Ba_4Fe_4ClO_{9.4(1)}$ leads to an average oxidation state of Fe to be 2.95, close to the theoretical maximum of 3.0 for iron.

While refining the structure of the crystal annealed at 800 °C in vacuum (group **II**), significant diffuse scattering (Fig. 2, group **II**) creates a big challenge to obtain a reliable refinement. In contrast to the [Ba–Cl–Ba] triplet ordering, which was successfully used, any attempt to apply the ordering of O atoms at $z = 0$ and 0.5 using the superspace approach was unsuccessful. Refinement in the supercell was unfeasible due to the number of refined parameters in the modulated structure which is $15 \times 15 = 225$ times larger than the unit cell of the average structure. Fig. 8c shows a comparison between the resulting supercell structure and the average structure. A statistical distribution of the O atoms
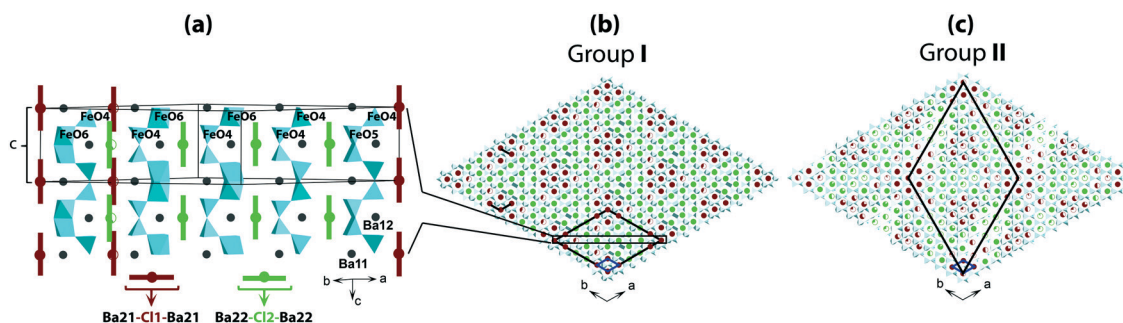

Fig. 8 Comparison of the commensurately modulated structures for $Ba_4Fe_4ClO_{9.5-x}$, group I and II crystals. Panels (a) and (b) show the (1–10) section and the structure projection along the hexagonal c-axis, respectively, for group I. Panel (c) shows the projection along the hexagonal c-axis for group II. In panels (b) and (c), only the centres of the Ba–Cl–Ba triplets, Cl1 (violet) and Cl2 (green), are shown to highlight the distribution of the triplets. Partially filled circles corresponding to Cl1 and Cl2 indicate a partial presence (disorder) of the triplets. This disorder increases in group II compared to group I. The blue and black rhombi represent the average cell and supercell, respectively, for groups I and II.

was used, and an anharmonic approximation of their atomic displacement was applied. The best result (Table S2†), which is only an approximation of the distribution of O atoms in the crystal structure of group **II**, confirms an increase in the disorder of [Ba–Cl–Ba] triplets in the channels (Fig. 7c). The corresponding CIF file is available with number 2127080.

The refinement of the modulated structure of crystals annealed under reducing conditions (group **III**) is still in progress. However, the refined composition gives an oxygen stoichiometry close to 9.0(1). It would imply that the average oxidation state of Fe is 2.75. 25% of the Fe^{3+} in the as-grown crystals was reduced to Fe^{2+}. From the refinement of the average structure, it can be claimed that the specific features of the modulated structure and its symmetry are due to partial ordering of the [Ba–Cl–Ba] triplets in the channels. In addition, although the composition of group **III** crystals is similar to that of the predicted non-modulated $Ba_4Fe_4ClO_9$ compound, the annealing of higher oxygen-stoichiometric crystals, under reducing conditions, does not yield crystals with an ordered structure.

Powder diffraction characteristics of $Ba_4Fe_4ClO_{9.5-x}$

For groups **I** and **II** compositions, theoretical powder XRD patterns were simulated using the models obtained from single-crystal XRD experiments. As shown in Fig. 9, the experimental patterns match quite well with the simulated ones. In addition, the powder XRD pattern of group **III** crystals is shown in Fig. S5.† The theoretical XRD patterns of the predicted ordered $Ba_4Fe_4ClO_8$ and $Ba_4Fe_4ClO_9$ are shown in Fig. S6.†
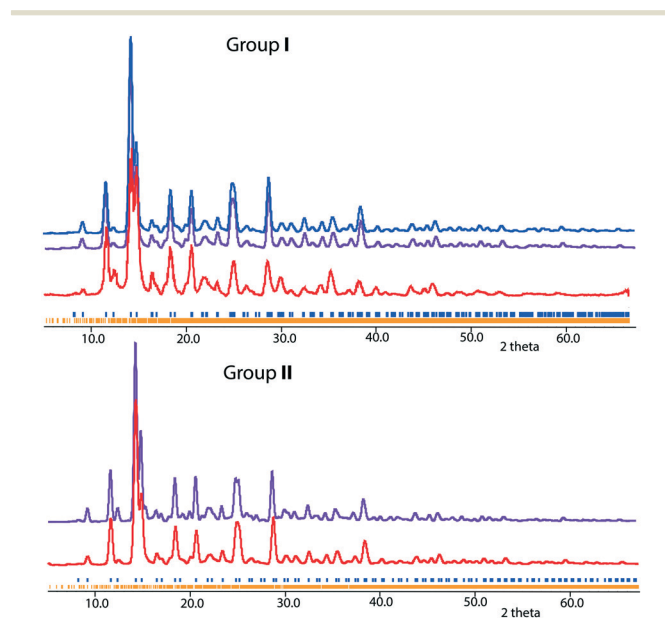

Fig. 9 Powder XRD patterns (Mo Kα radiation) of $Ba_4Fe_4ClO_{9.5-x}$ crystals belonging to groups **I** and **II**. The experimental (red) and simulated patterns using the superspace (blue) and supercell (violet) approximations are shown. The blue and orange strips at the bottom indicate the positions of the main and satellite reflections, respectively.

Summary and outlook

Summary

– We report on the synthesis of a new family of compounds, $Ba_4Fe_4ClO_{9.5-x}$, in which the oxygen stoichiometry and Fe oxidation state depend on the conditions of the crystal preparation as well as redox conditions during post-growth annealing.

– The framework of this hexagonal structure has the composition $Ba_2Fe_4O_{9.5-x}$ with x varying from experimentally obtained 0 to the theoretical prediction of 1.5. The structure forms open channels running parallel to the c-axis. The channels are filled with relatively mobile linear [Ba–Cl–Ba] triplets.

– Annealing the crystals in air, oxygen or vacuum at temperatures up to 600 °C does not influence the oxygen stoichiometry and oxidation state of the crystals. The composition of the crystals is found to be $Ba_4Fe_4ClO_{9.4(1)}$. However, these thermal treatments modify the structural modulation which originates in the oxygen distribution in the framework. Fe can be found in different coordination polyhedra (namely, FeO_4-tetrahedra, FeO_5-bipyramids, and FeO_6-octahedra). In the framework channels, linear [Ba–Cl–Ba] triplet distribution can be found to be partially ordered. Such a partial ordering is also responsible for the modulation found in the crystal structure of $Ba_4Fe_4ClO_{9.5-x}$.

– Annealing the crystals in $Ar-H_2$ reduces the oxygen stoichiometry. The resulting composition thus becomes $Ba_4Fe_4ClO_{9.0(1)}$. Fe is in a mixed oxidation state (1 Fe^{2+} and 3 Fe^{3+}). In addition to the lower O content, the structure of $Ba_4Fe_4ClO_9$ is characterized by a higher ordering of [Ba–Cl–Ba] triplets than in as-grown crystals or crystals annealed in vacuum, in air or in oxygen.

– Based on our presented results, the predicted ordered $Ba_4Fe_4ClO_8$ crystal structure will contain 3 Fe^{2+} and 1 Fe^{3+}. Iron atoms will be exclusively found in FeO_4 tetrahedra.

Outlook

The crystal growth and the post-growth annealing processes have induced modifications into the structure of $Ba_4Fe_4ClO_{9.5-x}$. This illustrates the flexibility of the crystal structure. The framework is stable with different polyhedra as well as with Fe^{2+} and Fe^{3+} in variable ratio. Therefore, the framework can vary from $[Ba_2Fe_4^{3+}O_8]^0$ or $[Ba_2Fe_4^{2+}O_8]^{4-}$ when built of FeO_4-tetrahedra only to $[Ba_2Fe_4^{3+}O_{12}]^{8-}$ or $[Ba_2Fe_4^{2+}O_{12}]^{12-}$ when built of FeO_6-octahedra only. In the channels created by the framework, fillers are mobile. The $[Ba-Cl-Ba]^{3+}$ triplets reported in the structure can potentially be substituted by other species with a charge varying between 0 and +12 to compensate the negative charge of the framework. From these perspectives, the discovery and description of the $Ba_4Fe_4ClO_{9.5-x}$ structure could be the first of a new family of compounds with similar framework, with a range of fillers in the channels and, therefore, variable chemical and physical properties.

Author contributions

Priya Ranjan Baral and Arnaud Magrez grew and annealed the crystals. Arnaud Magrez performed the XRF analysis. Wen-Hua Bi performed the single-crystal XRD experiments. The structure refinements were performed by Alla Arakcheeva. All authors wrote and commented on the paper.

Conflicts of interest

The authors declare no conflict of interest.

Acknowledgements

Notes and references

1 R. A. Singer, S. Monfette, D. Bernhardson, S. Tcyrulnikov, A. K. Hubbel and E. C. Hansen, *Org. Process Res. Dev.*, 2021, **25**, 1802.

2 L. Lv, M. Peng, L. Wu, Y. Dong, G. You, Y. Duan, W. Yang, L. He and X. Liu, *Nanoscale Res. Lett.*, 2021, **16**, 138.

3 W. Eerenstein, N. D. Mathur and J. F. Scott, *Nature*, 2006, **442**, 759.

4 A. Kreisel, P. J. Hirschfeld and B. M. Andersen, *Symmetry*, 2020, **12**(9), 1402.

5 M. Koltypin, S. Licht, I. Nowik, R. T. Vered, E. Levi, Y. Gofer and D. Aurbach, *J. Electrochem. Soc.*, 2006, **153**, A32.

6 I. Orlov, L. Palatinus, A. Arakcheeva and G. Chapuis, *Acta Crystallogr., Sect. B: Struct. Sci.*, 2007, **63**, 703.

7 A. V. Arakcheeva and O. G. Karpinskii, *Sov. Phys. - Crystallogr.*, 1990, **35**(5), 683.

8 NIST Inorganic Crystal Structure Database, *NIST Standard Reference Database Number 3*, National Institute of Standards and Technology, Gaithersburg MD, 20899, DOI: 10.18434/M32147, (retrieved [Dec. 07, 2021]). Details in https://icsd.nist.gov/guide.html.

9 S. Gražulis, A. Daškevič, A. Merkys, D. Chateigner, L. Lutterotti, M. Quirós, N. R. Serebryanaya, P. Moeck, R. T. Downs and A. LeBail, Crystallography Open Database (COD): an open-access collection of crystal structures and platform for world-wide collaboration, *Nucleic Acids Res.*, 2012, **40**, D420–D427, Details in https://wiki.crystallography.net/cod/citing/.

10 J. Zhang, A. Wolfel, L. Li, S. van Smaalen, H. L. Williamson and R. K. Kremer, *Phys. Rev. B: Condens. Matter Mater. Phys.*, 2012, **86**, 134428.

11 J. Wang, Y. Wen, H. Wang, H. H. Liu and X. Yang, *Prog. Chem.*, 2021, **33**(2), 263.

12 N. Abe, S. Shiozawa, K. Matsuura, H. Sagayama, A. Nakao, T. Ohhara, Y. Tokunaga and T. Arima, *Phys. Rev. B*, 2020, **101**, 180407(R).

13 L. Serrador, M. Hernando, J. L. Martinez, J. M. Gonzalez-Calbet, A. Varela, F. J. Garcia-Garcia and M. Parras, *Inorg. Chem.*, 2016, **55**, 6261.

14 A. Barman, G. Gubbiotti, S. Ladak, A. O. Adeyeye, M. Krawczyk, J. Grafe, C. Adelmann, S. Cotofana, A. Naeemi, V. I. Vasyuchka, B. Hillebrands, S. A. Nikitov, H. Yu, D. Grundler, A. V. Sadovnikov, A. A. Grachev, S. E. Sheshukova, J.-Y. Duquesne, M. Marangolo, G. Csaba, W. Porod, V. E. Demidov, S. Urazhdin, S. O. Demokritov, E. Albisetti, D. Petti, R. Bertacco, H. Schultheiss, V. V. Kruglyak, V. D. Poimanov, S. Sahoo, J. Sinha, H. Yang, M. Münzenberg, T. Moriyama, S. Mizukami, P. Landeros, R. A. Gallardo, G. Carlotti, J.-V. Kim, R. L. Stamps, R. E. Camley, B. Rana, Y. Otani, W. Yu, T. Yu, G. E. W. Bauer, C. Back, G. S. Uhrig, O. V. Dobrovolskiy, B. Budinska, H. Qin, S. van Dijken, A. V. Chumak, A. Khitun, D. E. Nikonov, I. A. Young, B. W. Zingsem and M. Winklhofer, *J. Phys.: Condens. Matter*, 2021, **33**, 413001.

15 Oxford Diffraction (2014), CrysAlisPRO. Agilent Technologies, Version 1.171.37.35 (release 13-08-2014 CrysAlis171.NET) (compiled Aug 13 2014, 18:06:01).

16 V. Petříček, M. Dusek and L. Palatinus, *Z. Kristallogr.*, 2014, **229**, 345.

17 L. Palatinus and G. Chapuis, *J. Appl. Crystallogr.*, 2007, **40**, 786.

18 Diamond – Crystal and Molecular Structure Visualization, Crystal Impact – Dr. H. Putz and Dr. K. Brandenburg GbR, Kreuzherrenstr. 102, 53227 Bonn, Germany, (see: https://www.crystalimpact.com/diamond/references.htm).

19 T. H. Stokes, B. J. Campbell and S. van Smaalen, *Acta Crystallogr., Sect. A: Found. Crystallogr.*, 2011, **67**, 45.